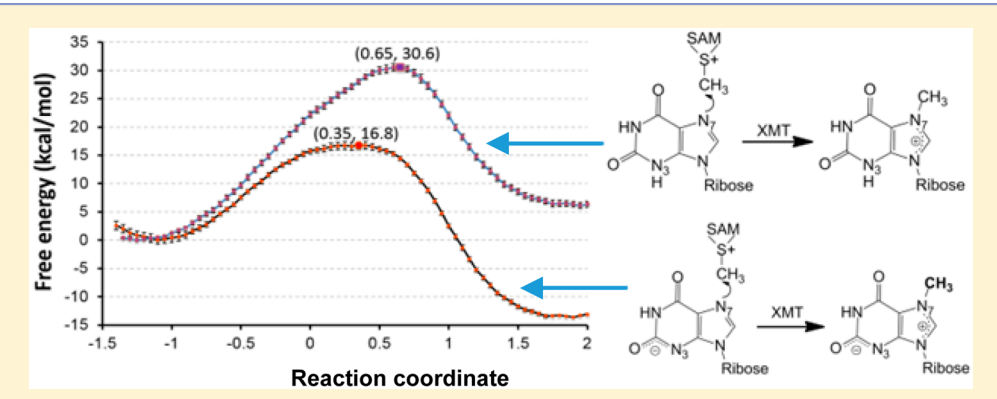
Understanding the Catalytic Mechanism of Xanthosine Methyltransferase in Caffeine Biosynthesis from QM/MM Molecular Dynamics and Free Energy Simulations

Ping Qian,*,†,‡,§ Hao-Bo Guo,†,∥ Yufei Yue,†,‡,∥ Liang Wang,§ Xiaohan Yang,¹ and Hong Guo*,†,‡

[⊥]Biosciences Division, Oak Ridge National Laboratory, Oak Ridge, Tennessee 37831, United States



ABSTRACT: S-Adenosyl-L-methionine (SAM) dependent xanthosine methyltransferase (XMT) is the key enzyme that catalyzes the first methyl transfer in the caffeine biosynthesis pathway to produce the intermediate 7-methylxanthosine (7mXR). Although XMT has been a subject of extensive discussions, the catalytic mechanism and nature of the substrate involved in the catalysis are still unclear. In this paper, quantum mechanical/molecular mechanical (QM/MM) molecular dynamics (MD) and free energy (potential of mean force or PMF) simulations are undertaken to determine the catalytic mechanism of the XMT-catalyzed reaction. Both xanthosine and its monoanionic form with N3 deprotonated are used as the substrates for the methylation. It is found that while the methyl group can be transferred to the monoanionic form of xanthosine with a reasonable free energy barrier (about 17 kcal/mol), that is not the case for the neutral xanthosine. The results suggest that the substrate for the first methylation step in the caffeine biosynthesis pathway is likely to be the monoanionic form of xanthosine rather than the neutral form as widely adopted. This conclusion is supported by the pK_a value on N3 of xanthosine both measured in aqueous phase and calculated in the enzymatic environment. The structural and dynamics information from both the X-ray structure and MD simulations is also consistent with the monoanionic xanthosine scenario. The implications of this conclusion for caffeine biosynthesis are discussed.

INTRODUCTION

The caffeine biosynthesis pathway produces two products, theobromine (3,7-dimethylxanthine or Tb) and caffeine (1,3,7-trimethylxanthine), that are important components in many beverages and pharmaceuticals. Caffeine is a purine alkaloid produced in some higher plants, including coffee, cacao and tea. The later stage of caffeine biosynthesis involves S-adenosyl-L-methionine dependent methyltransferases (MTs)^{1,2} that catalyze the three essential methylation steps with 7-methylxanthosine, 7-methylxanthine and theobromine formed as the intermediates during the processes.

The three methylation steps of caffeine biosynthesis begin with xanthosine (as the initial substrate) and end with caffeine (as the final product) with the action of three enzymes,

xanthosine MT (XMT), 7-methylxanthine MT (MXMT) and 3,7-dimethylxanthine MT(DXMT). The ribose on xanthosine is also removed under an as yet unclear mechanism.³ XMT catalyzes the methyl transfer from S-adenosyl-L-methionine (SAM) to the substrate xanthosine (XR), whereas DXMT can catalyze the methylation of the both 7mX(3-N) and Tb(1-N).³ XMT and DXMT are highly homologous to each other with more than 80% amino-acid sequence identity. The genome of Coffea canephora (Robusta coffee) has been recently sequenced,⁴ and the C. canephora genes that are the orthologs of the confirmed MT genes^{2,3} include the XMT gene (CcXMT)

Received: March 15, 2016



[†]Department of Biochemistry and Cellular and Molecular Biology, University of Tennessee, Knoxville, Tennessee 37996, United States

[‡]UT/ORNL Center for Molecular Biophysics, Oak Ridge National Laboratory, Oak Ridge, Tennessee 37830, United States

[§]Chemistry and Material Science Faculty, Shandong Agricultural University, Tai'an 271018, Shandong, People's Republic of China

Journal of Chemical Information and Modeling

Figure 1. Principal caffeine biosynthetic pathway involving xanthosine methyltransferase (XMT). 1,4 The first (1) step of the reaction involves the methylation of N7 of xanthosine. The second (2) step of the reaction involves the cleavage of ribose. It is generally adopted that the initial reactant is the neutral xanthosine, but the monoanionic form of xanthosine as a result of the dissociation of N3-H is also possible, as the corresponding pK_a value is 5.7 in aqueous phase from experimental measurement.

on chromosome 9, the MXMT gene (CcMXMT) on an unanchored scaffold, and the DXMT gene (CcDXMT) on chromosome 1. Comparative analysis of caffeine MTs demonstrated that these genes expanded through sequential tandem duplications independently of the genes from cacao and tea.4

The X-ray structures of XMT and DXMT from C. canephora are available,³ and these two structures can be superposed with an RMSD of only 1.1 Å. Nevertheless, each enzyme can only catalyze the methylation reaction involving its specific substrate(s), and question remains as to what are the factors that determine the substrate specificity for these enzymes. Our recent quantum mechanical/molecular mechanical study of DXMT⁵ showed that His160 at the enzyme's active site is likely to play a role as a general base/acid for the methyl transfer process. This result seems to provide an explanation concerning the experimental observations that XMT has no activity on 7mX or Tb.⁶ Indeed, the corresponding residue in XMT is Gln161, which may have hydrogen bonding potential for substrate binding but is less likely to pay a role of a general acid/base catalyst. Our earlier simulation results seem to be consistent with the experimental data that for the xanthosine methyltransferase CmXRS1, the mutants that showed 3-N methylation activity and produced caffeine from paraxanthine were all found to possess the $Gln161 \rightarrow His$ replacement.

XMT (studied in this work) is capable of catalyzing methylation of the substrate xanthosine to produce 7methylxanthosine (7mXR), and the enzyme is active at pH 7.9.3 It is generally assumed that N3 of xanthosine remains protonated during the methylation process. 1-7 However, the pK_a value of N3 suggests that it may be deprotonated in the enzyme (Figure 1 and see below). Thus, whether the neutral xanthosine or its monoanionic form with N3 deprotonated is the true substrate for the first methylation step is still not clear. Understanding this question may be of importance for determination of the mechanisms of other enzyme-catalyzed reactions in the caffeine biosynthesis pathway as well. Here molecular dynamics (MD) and free energy (potential of mean force or PMF) simulations with quantum mechanical/ molecular mechanical (QM/MM) potentials were undertaken

for understanding the XMT-catalyzed reaction. Both xanthosine and its monoanionic form with N3 deprotonated were used as the substrates for the methylation process. It was found that the methyl group could be transferred to the monoanionic form with a relatively low free energy barrier (~17 kcal/mol). By contrast, the free energy barrier (~31 kcal/mol) for the methylation of the neutral xanthosine is significantly higher. This result suggests that the substrate for the first methyl transfer in the caffeine biosynthesis pathway is likely to be the monoanionic form of xanthosine. This is consistent with the pK_a values of xanthosine at N3 in solution (i.e., $pK_a = 5.7$ from the experiment measurement⁸ and 5.0 based on the calculations of this work) and at the enzyme active site (i.e., $pK_a = 1.8$ based on the calculations from this work). The conclusion is also supported by a detailed examination of the X-ray structure and comparison of the reactant structures of XMT complexed with the two different forms of the substrate obtained from the MD and free energy simulations. The implications of this work are discussed.

METHODS

The QM/MM MD and PMF simulations were undertaken in the determination of the free energy profiles for the methyl transfer from SAM to N7 on xanthosine (XR hereafter) and for the characterization of the active site dynamics using the CHARMM program. 9,10 The whole substrate and -CH₂-CH₂-S⁺(Me)-CH₂- part of SAM were treated by QM. For the rest of the system, molecular mechanics (MM or force filed) was used. CHARMM force field (PARAM27)11 was applied for the molecular mechanics region, and SCC-DFTB, a self-consistent charge density functional tight-binding method, 12,13 was used for the QM region. To separate the QM and MM region, the link-atom approach 14 implemented in CHARMM was adopted. The reliability of SCC-DFTB has been tested for the similar methylation reaction in our earlier study by comparing the SCC-DFTB and high-level MP2/6-31G** results. It was demonstrated that SCC-DFTB performed reasonably well. For the solvent molecules, a modified TIP3P water model¹⁵ was used. The simulations were based on the stochastic boundary molecular dynamics method, ¹⁶ which divides the system into a reservoir region and a reaction zone (which contained a reaction region and a buffer region). For the reaction region, a sphere with radius r of 20 Å was used, and for the buffer region, r was in the range 20 Å $\leq r \leq$ 22 Å. The C5 (N7) atom of the monoanionic (neutral) form of substrate is the reference center for partitioning the system. The number of atoms in the resulting systems is about 5800, including those from about 600 water molecules.

The crystallographic complex (PDB ID: 2EG5) of XMT with S-adenosyl-L-homocysteine (SAH) and XR³ was used for the initial coordinates. A methyl group was built manually on S_{δ} of SAH to form SAM, the methyl-donor. Hydrogen atoms of XMT were built with the HBUILD module 17 in the CHARMM program. The initial structures were optimized for the entire stochastic boundary systems with the steepest descent (SD) and adopted-basis Newton-Raphson (ABNR) methods. The systems were gradually heated from 50.0 to 298.15 K in 50 ps. The time step for the integration of equation of motion was 1 fs, and the coordinates were saved every 50 fs for analyses. For each of the systems, the total QM/MM MD runs reach 5 ns. The umbrella sampling method 18,19 was then applied along with the weighted histogram analysis method (WHAM) for the determination of the free energy change along the reaction coordinate for the methyl transfer from SAM to N7 of either a neutral XR or the monoanionic XR deprotonated at N3. The reaction coordinate used in this study is the linear combination of $r(C_M - N_7)$ and $r(C_M - S_\delta)$ $[R = r(C_M - S_\delta) - r(C_M - S_\delta)]$ N_7)]. For the methylation process, 18 simulation windows were performed. Each window comprises a 100 ps production run after an equilibration run for 50 ps. For the PMF simulations, the force constant used for the harmonic biasing potentials is 400 kcal $\text{mol}^{-1} \text{ Å}^{-2}$. For each of the two systems with neutral or monoanionic substrate, five independent PMF simulations were undertaken. The free energies (PMFs) and statistical errors were taken as the average values and standard deviations from the five runs, respectively.

The pK_a values at N3 of XR in aqueous phase and at the enzyme's active site were calculated using PROPKA3.1. The pK_a value in the aqueous phase was calculated to be 4.97, in a reasonable agreement with the experimental value ($pK_a = 5.70$). This result confirms that the pK_a prediction from PROPKA3.1 is meaningful. The whole protein structure was used for the pK_a calculation, resulted in a pK_a value of 1.83 at N3, which is even lower than the values in the aqueous phase. The results support the suggestion that XR is deprotonated at N3 in the protein environment as well.

RESULTS AND DISCUSSIONS

1. Analysis of the X-ray Structure of the XMT Complex and Reactant Structures Involved in the N7 Methylation. The active site of the X-ray structure for the XMT complex is plotted in Figure 2A. As is apparent from Figure 2A, N7 of XR is located near S_{δ} of SAH with an $r(S_{\delta}\cdots N7)$ distance of 4.03 Å, consistent with the fact that the N7 atom is the methyl-acceptor. There are several hydrogen bonds between XR and the enzyme, which may make important contributions to the substrate binding. It is of interest to note that two relatively strong hydrogen bonds (H-bonds) are formed between the hydroxyl groups of Tyr321 and Tyr356 of XMT and O2 of the purine ring, whereby the H-bond distances between the corresponding oxygen atoms are 2.79 and 2.43 Å, respectively. The H-bond distance of 2.43 Å between non-hydrogen atoms is significantly shorter than those for normal

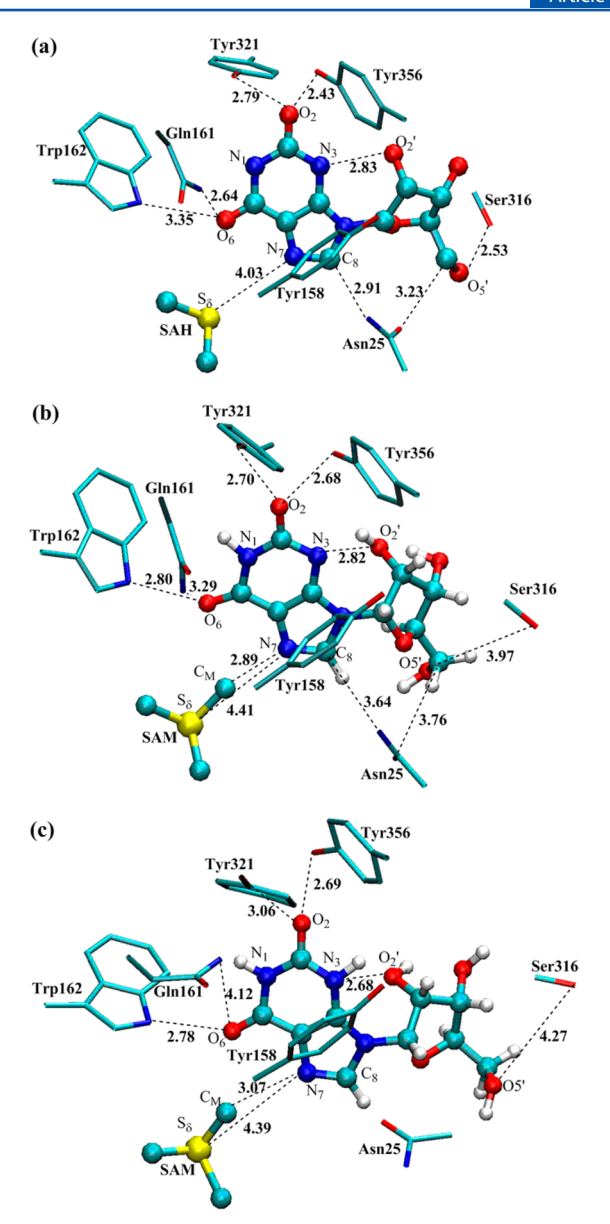


Figure 2. (a) Active-site structure of the XMT complex containing SAH and xanthosine (XR) based on the crystal structure (PDB ID: 2EG5).3 XMT was plotted in sticks, and SAH and xanthosine were in balls and sticks. Only the residues that are close to xanthosine and the three atoms, C5', CG, and S_{δ} , from SAH are shown for clarity. Some distances are also given (in angstroms). (b) Representative structure for the active-site of the reactant complex containing SAM and XR with N3 deprotonated (i.e., the monoanionic form of XR) from the QM/MM molecular dynamics simulations. The average distances involving some atoms (residues) are shown that are based on the trajectories between 2 ns and 5 ns within the 5 ns simulations performed in this work. (c) Representative structure for the active-site of the reactant complex containing SAM and the neutral XR (i.e., with N3 protonated) from the QM/MM molecular dynamics simulations. The average distances involving the same atoms are also given (except the one involving Asn25).

hydrogen bonds (~3.0 Å). The short and strong hydrogenbonds are known to be often associated with negatively charged oxygen acceptors, consistent with the suggestion that XR might be deprotonated at N3 (see Figure 1). Figure 2A also shows that Trp162 and Gln161 form hydrogen bonds to O6 of XR. In DXMT, His160 replaces Gln161 and forms an H-bond to the O2 atom of theobromine or 7mX. Our previous QM/MM simulations⁵ suggested that His160 is likely to play a role as a general base/acid in the DXMT-catalyzed methylation reaction. This suggestion seems to be consistent with the experimental data, which showed that for the xanthosine methyltransferase CmXRS1, the mutants with the 3-N methylation activity and producing caffeine from paraxanthine were all found to possess the Gln161 → His replacement. An H-bond is formed between Ser-316 and the O5' hydroxyl group from the ribose moiety of XR; the residue corresponding to Ser-316 in DXMT is Val. It has been proposed that Ser316 might be essential for the XMT substrate specificity.3 The O2' hydroxyl group from the ribose moiety forms an H-bond with the N3 atom of the purine ring (the corresponding H-bond distance is ~2.83 Å). Because hydrogen atoms in the X-ray structure are invisible, question remains as to whether the O2' hydroxyl group acts as the hydrogen bond donor with N3 deprotonated or hydrogen bond acceptor with N3 protonated. Besides the hydrogen bonding interactions, hydrophobic interactions also exist in the active site. For example, XR is involved in hydrophobic interactions with Tyr24 and Val320 (not shown). It is of interest to note from Figure 2A that the phenyl ring of Tyr158 is located nearly perpendicular to the purine ring with the edge of the aromatic ring pointing to the substrate, an indication that the anionquadrupole interaction might be involved in the substrate binding. 21,22

The representative structure for the active-site of the reactant complex containing the deprotonated XR in XMT based on 5 ns QM/MM MD simulation is plotted in Figure 2B. Examination of the structures in Figure 2A,B shows that the H-bond and hydrophobic interactions that exist in the crystal structure generally remain in the reactant complex involving the deprotonated XR. For instance, the two strong H-bonds between O2 and the Tyr321/Tyr356 hydroxyl groups also exist in the structure from the simulations, and Trp162 and Gln161 still form hydrogen bonds to O6. Moreover, the phenyl ring of Tyr158 remains nearly perpendicular to the purine ring with the edge of the aromatic ring pointing to the substrate. As is shown in Figure 2B, the O2' hydroxyl group from the ribose moiety donates a hydrogen bond to N3 of the purine ring; the average H-bond distance is 2.82 Å that is basically the same as the H-bond distance (2.83 Å) observed in the crystal structure. As is expected, some small deviations from the X-ray structure were observed (e.g., the hydrogen bond distance involving Ser316 is changed from 2.53 to 3.97 Å). This seems reasonable, as the reactant complex contains SAM, whereas the crystal structure contains SAH. The positively charged SAM is likely to modify the X-ray structure containing SAH.

The representative structure for the active-site of the reactant complex containing the neutral XR based on the 5 ns MD simulations is plotted in Figure 2C. Figure 2C shows that the interactions and the substrate conformation have been changed considerably from those in the crystal structure if N3 is protonated. Indeed, the hydrogen bond involving Gln161 in the crystal structure is basically broken and that involving Tyr321 seems to be weakened (based on the increase of the hydrogen bond distance). The orientation of Tyr158 relative to the substrate is somehow changed for the neutral substrate compared to the crystal structure. One of the most significant changes in XMT complexed with the neutral substrate from the crystal structure involves the ribose moiety. Indeed, the –CH₂–OS′–H chain of the ribose moiety has undergone a conformational change, leading to a different configuration

compared to that in the crystal structure. The interactions involving Ser316 and Asn25 observed in the crystal structure are also broken (>4 Å). This change of the XR conformation might be due in part to the fact that the O2' hydroxyl group now accepts an H-bond from the N3–H group of the purine ring in the neutral substrate rather than donating an H-bond to the N3 atom of the purine ring in the monoanionic form of the substrate (Figure 2B).

The results reported here demonstrate that XR with N3 deprotonated (i.e., the monoanionic form) is more likely to be the true substrate for the XMT-catalyzed reaction, as the average structure for its complex with XMT obtained from the simulations seems to be more consistent with the available experimental structure. As will be shown in the next section, this suggestion is further supported by the results of the free energy (potential of mean force) simulations.

2. Free Energy (PMF) Simulations of the Methylation of XR with N3 Deprotonated and Protonated, Respectively. As is evident from Figure 2B,C, the average $r(C_M \cdots N7)$ distances in the reactant complexes are about 3 Å in the MD simulations, and the methyl group of SAM and the lone-pair electrons of N7 can be well aligned for both deprotonated and neutral XR. As was suggested from previous studies, $^{23-28}$ such a good alignment may be of importance for an efficient methyl transfer, at least in some cases. Nevertheless, as will be shown below, the methyl transfer from SAM to the anionic XR seems to be far more efficient than that to the neutral XR based on our free energy simulations, even though the near attack configuration can also be formed for the neutral XR.

The PMF curves obtained from the QM/MM free energy simulations are compared in Figure 3 for the methyl transfers

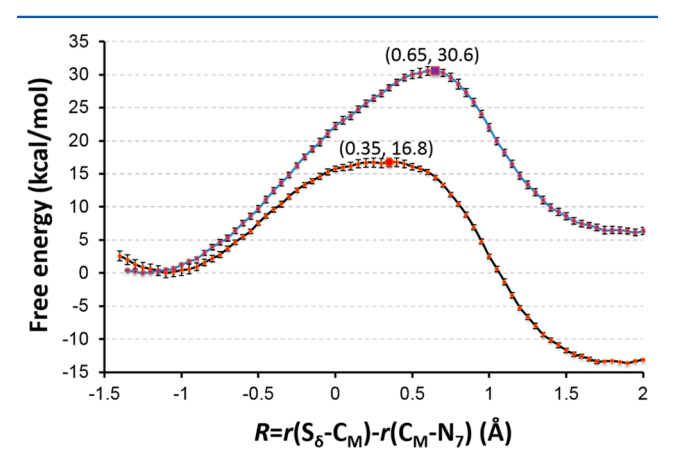


Figure 3. Free energy (potential of mean force) profiles for the methyl transfers from SAM to N7 of the deprotonated and neutral XR in XMT, respectively, as a function of $R = r(C_M \cdots S_\delta) - r(C_M \cdots N_7)$ (reaction coordinate) along with the statistical errors generated from the PMF simulations. The black line: the methyl transfer from SAM to N7 of the deprotonated XR. The blue line: the methyl transfer from SAM to N7 of the neutral XR. The value of reaction coordinate and the free energy barrier near the transition state are given as the first and second numbers, respectively, in the parentheses for each reaction.

involving the deprotonated and neutral XR, respectively. As is shown from Figure 3, the free energy barriers for the methyl transfer from SAM to the monoanionic and neutral XR are 16.8 and 30.6 kcal/mol, respectively. Thus, for XR with N3 deprotonated the free energy barrier is as much as 14 kcal/mol lower compared to that for the neutral XR, suggesting that the true substrate for the first methylation step is likely to be

the monoanionic form of XR. This conclusion is consistent with p $K_{\rm a}$ value at N3 of XR both detected in aqueous phase (5.7)⁸ and calculated in the enzymatic environment using PROPKA3.1²⁰ (1.83). The results based on our PMF simulations are also consistent with the reactant structures from the QM/MM MD simulations discussed earlier. Indeed, the average XMT structure containing the monoanionic form is more consistent with the crystal structure than that containing the neutral XR. It is of interest to note from Figure 3 that the transition state for the XMT complex containing the monoanionic form is reached at around $R \sim 0.35$ Å compared to $R \sim 0.65$ Å reached by the complex containing the neutral XR.

Representative structures for the XMT complexes from the PMF simulations during the methyl transfer to the monoanionic form are shown in Figure 4. As is clear from Figure 4, the H-bond and hydrophobic interactions in the reactant state, transition state and product state do not have significant changes and are rather similar to those obtained from the X-ray structure. For example, the H-bond between Gln161 and O6 is stable and only changed from 3.11 to 2.99 Å as the methylation reaction proceeds from the near reactant to near transition state. As is in the case of DXMT, 5 the hydrogen bond between Trp162 and O6 is well maintained at around 2.8 Å. Moreover, the hydrogen bonding interactions involving Tyr321 and Tyr356 and the interaction involving Tyr158 are generally stable. These interactions presumably help to maintain the conformation of the XMT complex and contribute to the relatively low free energy barrier (~16.8 kcal/mol) for the methyl transfer. In contrast, larger changes were observed in the active site of the XMT complex containing the neutral XR during the free energy simulations of the methylation process (Figure 5). For example, the average hydrogen bond distance between Tyr321 and O2 increased from 2.85 Å in near reactant state to 3.36 Å in near transition state; the hydrogen bond strength is expected to be weakened accordingly. Interestingly, the hydrogen bond between Tyr321 and N1 decreases from 3.60 Å in near reactant state to 3.13 Å in near transition state, indicating a potential strengthening of this interaction.

3. Implications for the XMT-Catalyzed Reaction. The methyl transfer from SAM to N7 of the XR substrate is the first methylation step of caffeine biosynthesis. During this process, the lone pair of electrons on N7 attacks C_M of the methyl group of SAM in a $S_N 2$ substitution mechanism. One of the key questions for this methylation process is the protonation state of XR. It has generally been assumed that the substrate is neutral with N3 of XR protonated during the methylation process. $^{1,3-7}$ This seems to be inconsistent with the experiments 8 that showed a relatively low p K_a of 5.7 at N3. Thus, for the neutral form of XR to be the substrate of XMT a general acid catalyst (presumably from an enzyme) should first protonate N3, followed by the XMT catalysis that transfer XR to 7-methylxanthosine (in a monocationic form; see Figure 1). However, such a general acid catalyst has never been identified.

The other scenario is that the monoanionic form of XR abundant in solution would bind to the XMT active site, and the enzyme directly catalyzes its transformation into the neutral form of 7-methylxanthosine. The monoanionic form of XR is confirmed by the pK_a calculations in the protein environment in the present work. We also compared the reactant structures of the XMT complexes (containing the two different forms of the substrate) obtained from the simulations with the crystal

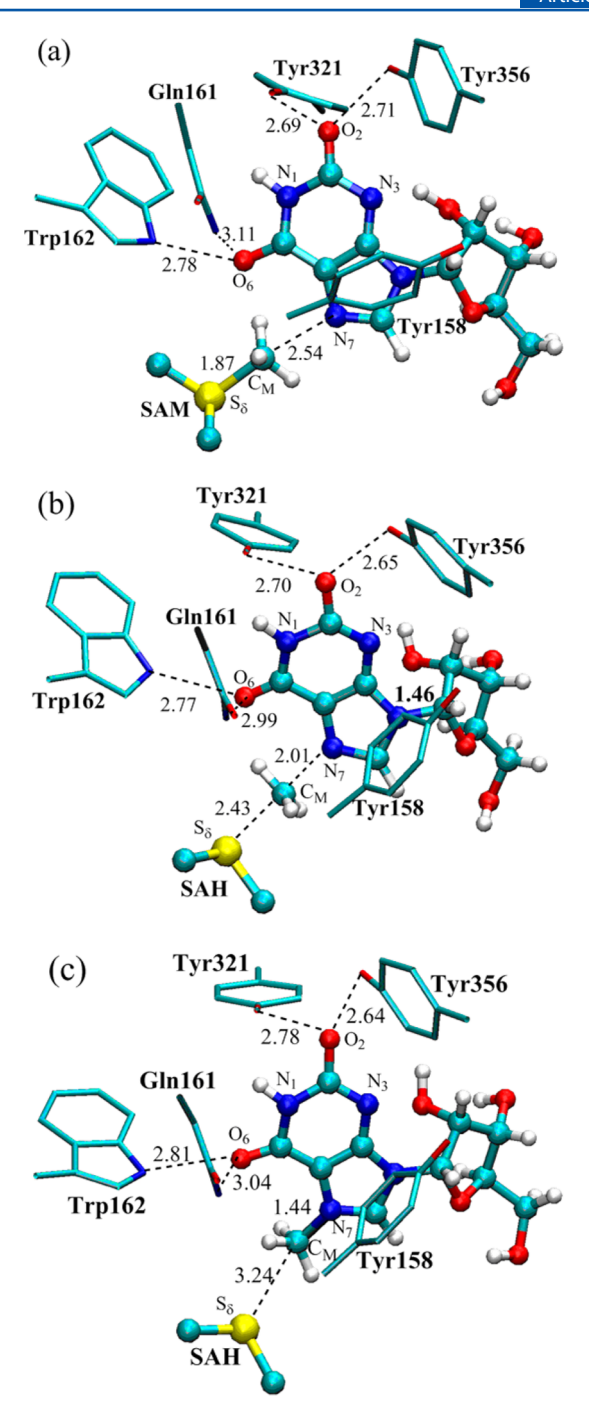


Figure 4. (a) Representative structure of the active site near the reactant (i.e., obtained from Window 5) from the PMF simulations for the methylation of the monoanionic form of XR. Some average distances for the H-bonds from the monoanionic form of XR to the nearby residues are shown (in angstroms). (b) Representative structure of the active site near transition state (Window 10) for the methylation of N7. (c) Representative structure of the active site near product (Window 17) after the methylation of N7.

structure. The results demonstrate that xanthosine with N3 deprotonated (i.e., the monoanionic form) is more likely to be the true substrate for the XMT-catalyzed reaction, as the average structure for the corresponding XMT complex is more likely to represent the crystallographic structure. This scenario is further supported by the results from the free energy (PMF) simulations. Indeed, it was demonstrated that the methyl

Journal of Chemical Information and Modeling

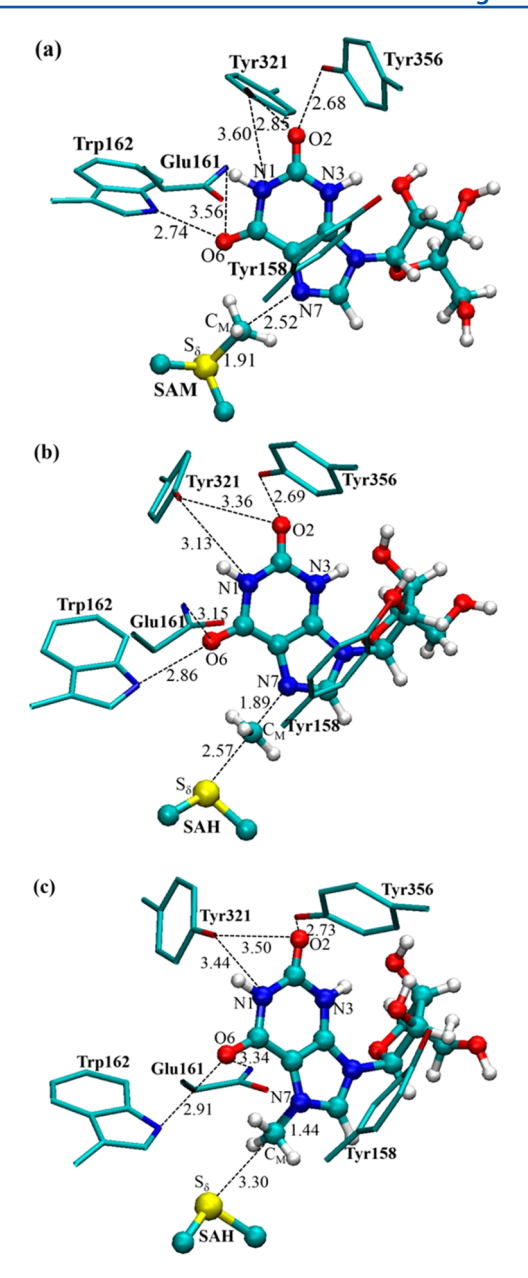


Figure 5. (a) Representative structure of the active site near the reactant (i.e., obtained from Window 5) from the PMF simulations for the methylation of the neutral XR. Some average distances for the hydrogen bonds between the neutral XR and nearby residues are shown (in angstroms). (b) Representative structure of the active site near transition state (Window 11) for the methylation of N7. (c) Representative structure of the active site near product (Window 17) after the methylation of N7.

transfer reaction for the N3-deprotonated-XR in XMT has a free energy barrier that is ~14 kcal/mol lower than the free energy barrier involving the neutral XR.

Determination of the true substrate for the XMT-catalyzed reaction may have implications for determining the reaction mechanisms of the caffeine biosynthesis pathway. For instance, one of the mysterious observations³ is that 7mX was the only detectable product from the first methylation step, leading to a hypothesis that XMT might be able to catalyze the nucleotide cleavage as well. Because the product from the XMT-catalyzed methyl-transfer reaction may serve as be the reactant for the nucleotide cleavage, identification of the true product (i.e., the

neutral versus monocationic forms of 7-methylxanthosine) is crucial for determining whether this potential mechanism is feasible or not in future studies.

CONCLUSIONS

It is generally adopted that N3 of xanthosine remains protonated during the methylation process catalyzed by XMT in the caffeine biosynthesis pathway. Here, computer simulations have been undertaken for understanding the XMT-catalyzed reaction and for determining the nature of the substrate. It was found that while the free energy barrier (~17 kcal/mol) for the methyl transfer to the monoanionic form of xanthosine is reasonable for the enzyme-catalyzed reaction, the barrier involving the neutral xanthosine (~31 kcal/mol) is significantly higher. Thus, for the caffeine biosynthesis pathway the substrate for its first methylation step is likely to be the monoanionic form of xanthosine. This conclusion agrees with the experimental pK_a detection in aqueous phase⁸ and the pK_a calculation in the enzymatic environment, such that N3 of XR should be in a deprotonated state at physiological pH. The examination of the reactant structures of XMT complexed with the two different forms of the substrate (i.e, the monoanionic versus neutral forms of xanthosine) showed that although the hydrogen bonding and hydrophobic interactions involving the monoanionic form closely represent the corresponding interactions in the crystal structure, this seems not to be the case for the reactant complex involving the neutral XR. Therefore, the structural analysis also supports our proposal that xanthosine with N3 deprotonated should be the true substrate for XMT.

AUTHOR INFORMATION

Corresponding Authors

*H. Guo. E-mail: hguo1@utk.edu; Fax: +1(865)974-6306. *P. Qian. E-mail: qianp@sdau.edu.cn.

Author Contributions

Equal contribution.

Notes

The authors declare no competing financial interest.

ACKNOWLEDGMENTS

This work was supported in part by grants 0817940 from the National Science Foundation (H.G.). Oak Ridge National Laboratory is managed by UT-Battelle, LLC for the U.S. Department of Energy under contract number DE-AC05-00OR22725. This work used the Extreme Science and Engineering Discovery Environment (XSEDE), which is supported by National Science Foundation grant number ACI-1053575. The research has been aided by the National Nature Science Foundation of China (No. 20903063 to P.Q.), the grant from the Postdoctoral Foundation of Shandong Agricultural University in China (No. 76335 to P.Q.) and China Scholarship Council (No. 201408370020 to P.Q.).

REFERENCES

- (1) Ashihara, H.; Sano, H.; Crozier, A. Caffeine and Related Purine Alkaloids: Biosynthesis, Catabolism, Function and Genetic Engineering. Phytochemistry 2008, 69, 841-856.
- (2) Ashihara, H.; Zheng, X. Q.; Katahira, R.; Morimoto, M.; Ogita, S.; Sano, H. Caffeine Biosynthesis and Adenine Metabolism in Transgenic Coffea Canephora Plants with Reduced Expression of N-Methyltransferase Genes. Phytochemistry 2006, 67, 882-886.

- (3) McCarthy, A. A.; McCarthy, J. G. The Structure of Two N-Methyltransferases from the Caffeine Biosynthetic Pathway. *Plant Physiol.* **2007**, *144*, 879–889.
- (4) Denoeud, F.; Carretero-Paulet, L.; Dereeper, A.; Droc, G.; Guyot, R.; Pietrella, M.; Zheng, C.; Alberti, A.; Anthony, F.; Aprea, G.; Aury, J.-M.; Bento, P.; Bernard, M.; Bocs, S.; Campa, C.; Cenci, A.; Combes, M.-C.; Crouzillat, D.; Da Silva, C.; Daddiego, L.; De Bellis, F.; Dussert, S.; Garsmeur, O.; Gayraud, T.; Guignon, V.; Jahn, K.; Jamilloux, V.; Joet, T.; Labadie, K.; Lan, T.; Leclercq, J.; Lepelley, M.; Leroy, T.; Li, L.-T.; Librado, P.; Lopez, L.; Munoz, A.; Noel, B.; Pallavicini, A.; Perrotta, G.; Poncet, V.; Pot, D.; Priyono; Rigoreau, M.; Rouard, M.; Rozas, J.; Tranchant-Dubreuil, C.; VanBuren, R.; Zhang, Q.; Andrade, A. C.; Argout, X.; Bertrand, B.; de Kochko, A.; Graziosi, G.; Henry, R. J.; Jayarama; Ming, R.; Nagai, C.; Rounsley, S.; Sankoff, D.; Giuliano, G.; Albert, V. A.; Wincker, P.; Lashermes, P. The Coffee Genome Provides Insight into the Convergent Evolution of Caffeine Biosynthesis. *Science* 2014, 345, 1181–1184.
- (5) Yue, Y.; Guo, H. Quantum Mechanical/Molecular Mechanical Study of Catalytic Mechanism and Role of Key Residues in Methylation Reactions Catalyzed by Dimethylxanthine Methyltransferase in Caffeine Biosynthesis. J. Chem. Inf. Model. 2014, 54, 593–600.
- (6) Mizuno, K.; Kato, M.; Irino, F.; Yoneyama, N.; Fujimura, T.; Ashihara, H. The First Committed Step Reaction of Caffeine Biosynthesis: 7-Methylxanthosine Synthase Is Closely Homologous to Caffeine Synthases in Coffee (Coffea Arabica L.). FEBS Lett. 2003, 547, 56–60.
- (7) Mizuno, K.; Kurosawa, S.-i.; Yoshizawa, Y.; Kato, M. Essential Region for 3-N Methylation in N-Methyltransferases Involved in Caffeine Biosynthesis. Z. Naturforsch., C: J. Biosci. 2010, 65, 257–265.
- (8) Kulikowska, E.; Kierdaszuk, B.; Shugar, D. Xanthine, Xanthosine and Its Nucleotides: Solution Structures of Neutral and Ionic Forms, and Relevance to Substrate Properties in Various Enzyme Systems and Metabolic Pathways. *Acta Biochim. Polym.* **2004**, *51*, 493–531.
- (9) Brooks, B. R.; Brooks, C. L., III; Mackerell, A. D., Jr.; Nilsson, L.; Petrella, R. J.; Roux, B.; Won, Y.; Archontis, G.; Bartels, C.; Boresch, S.; Caflisch, A.; Caves, L.; Cui, Q.; Dinner, A. R.; Feig, M.; Fischer, S.; Gao, J.; Hodoscek, M.; Im, W.; Kuczera, K.; Lazaridis, T.; Ma, J.; Ovchinnikov, V.; Paci, E.; Pastor, R. W.; Post, C. B.; Pu, J. Z.; Schaefer, M.; Tidor, B.; Venable, R. M.; Woodcock, H. L.; Wu, X.; Yang, W.; York, D. M.; Karplus, M. Charmm: The Biomolecular Simulation Program. *J. Comput. Chem.* **2009**, *30*, 1545–1614.
- (10) Brooks, B. R.; Bruccoleri, R. E.; Olafson, B. D.; States, D. J.; Swaminathan, S.; Karplus, M. Charmm a Program for Macromolecular Energy, Minimization, and Dynamics Calculations. *J. Comput. Chem.* **1983**, *4*, 187–217.
- (11) MacKerell, A. D.; Bashford, D.; Bellott, M.; Dunbrack, R. L.; Evanseck, J. D.; Field, M. J.; Fischer, S.; Gao, J.; Guo, H.; Ha, S.; Joseph-McCarthy, D.; Kuchnir, L.; Kuczera, K.; Lau, F. T. K.; Mattos, C.; Michnick, S.; Ngo, T.; Nguyen, D. T.; Prodhom, B.; Reiher, W. E.; Roux, B.; Schlenkrich, M.; Smith, J. C.; Stote, R.; Straub, J.; Watanabe, M.; Wiorkiewicz-Kuczera, J.; Yin, D.; Karplus, M. All-Atom Empirical Potential for Molecular Modeling and Dynamics Studies of Proteins. *J. Phys. Chem. B* 1998, 102, 3586–3616.
- (12) Cui, Q.; Elstner, M.; Kaxiras, E.; Frauenheim, T.; Karplus, M. A Qm/Mm Implementation of the Self-Consistent Charge Density Functional Tight Binding (Scc-Dftb) Method. *J. Phys. Chem. B* **2001**, 105, 569–585.
- (13) Elstner, M.; Porezag, D.; Jungnickel, G.; Elsner, J.; Haugk, M.; Frauenheim, T.; Suhai, S.; Seifert, G. Self-Consistent-Charge Density-Functional Tight-Binding Method for Simulations of Complex Materials Properties. *Phys. Rev. B: Condens. Matter Mater. Phys.* 1998, 58, 7260–7268.
- (14) Field, M. J.; Bash, P. A.; Karplus, M. A Combined Quantum-Mechanical and Molecular Mechanical Potential for Molecular-Dynamics Simulations. *J. Comput. Chem.* **1990**, *11*, 700–733.
- (15) Jorgensen, W. L.; Chandrasekhar, J.; Madura, J. D.; Impey, R. W.; Klein, M. L. Comparison of Simple Potential Functions for Simulating Liquid Water. *J. Chem. Phys.* **1983**, *79*, 926–935.

- (16) Brooks, C. L.; Brunger, A.; Karplus, M. Active-Site Dynamics in Protein Molecules a Stochastic Boundary Molecular-Dynamics Approach. *Biopolymers* **1985**, *24*, 843–865.
- (17) Brunger, A. T.; Karplus, M. Polar Hydrogen Positions in Proteins Empirical Energy Placement and Neutron-Diffraction Comparison. *Proteins: Struct., Funct., Genet.* **1988**, *4*, 148–156.
- (18) Kumar, S.; Bouzida, D.; Swendsen, R. H.; Kollman, P. A.; Rosenberg, J. M. The Weighted Histogram Analysis Method for Free-Energy Calculations on Biomolecules 0.1. The Method. *J. Comput. Chem.* **1992**, *13*, 1011–1021.
- (19) Torrie, G. M.; Valleau, J. P. Monte-Carlo Free-Energy Estimates Using Non-Boltzmann Sampling Application to Subcritical Lennard-Jones Fluid. *Chem. Phys. Lett.* **1974**, *28*, 578–581.
- (20) Sondergaard, C. R.; Olsson, M. H.; Rostkowski, M.; Jensen, J. H. Improved Treatment of Ligands and Coupling Effects in Empirical Calculation and Rationalization of Pka Values. *J. Chem. Theory Comput.* **2011**, *7*, 2284–2295.
- (21) Jackson, M. R.; Beahm, R.; Duvvuru, S.; Narasimhan, C.; Wu, J.; Wang, H.-N.; Philip, V. M.; Hinde, R. J.; Howell, E. E. A Preference for Edgewise Interactions between Aromatic Rings and Carboxylate Anions: The Biological Relevance of Anion-Quadrupole Interactions. *I. Phys. Chem. B* **2007**, *111*, 8242–8249.
- (22) Philip, V.; Harris, J.; Adams, R.; Nguyen, D.; Spiers, J.; Baudry, J.; Howell, E. E.; Hinde, R. J. A Survey of Aspartate-Phenylalanine and Glutamate-Phenylalanine Interactions in the Protein Data Bank: Searching for Anion-Pi Pairs. *Biochemistry* **2011**, *50*, 2939–2950.
- (23) Yao, J.; Xu, Q.; Chen, F.; Guo, H. Qm/Mm Free Energy Simulations of Salicylic Acid Methyltransferase: Effects of Stabilization of Ts-Like Structures on Substrate Specificity. *J. Phys. Chem. B* **2011**, 115, 389–396.
- (24) Guo, H.-B.; Guo, H. Mechanism of Histone Methylation Catalyzed by Protein Lysine Methyltransferase Set7/9 and Origin of Product Specificity. *Proc. Natl. Acad. Sci. U. S. A.* **2007**, *104*, 8797—8802.
- (25) Zhang, X.; Bruice, T. C. Catalytic Mechanism and Product Specificity of Rubisco Large Subunit Methyltransferase: Qm/Mm and Md Investigations. *Biochemistry* **2007**, *46*, 5505–5514.
- (26) Hu, P.; Wang, S.; Zhang, Y. How Do Set-Domain Protein Lysine Methyltransferases Achieve the Methylation State Specificity? Revisited by Ab Initio Qm/Mm Molecular Dynamics Simulations. *J. Am. Chem. Soc.* **2008**, *130*, 3806–3813.
- (27) Yao, J.; Chu, Y.; An, R.; Guo, H. Understanding Product Specificity of Protein Lysine Methyltransferases from Qm/Mm Molecular Dynamics and Free Energy Simulations: The Effects of Mutation on Set7/9 Beyond the Tyr/Phe Switch. *J. Chem. Inf. Model.* **2012**, *52*, 449–456.
- (28) Chu, Y.; Li, G.; Guo, H. Qm/Mm Md and Free Energy Simulations of the Methylation Reactions Catalyzed by Protein Arginine Methyltransferase Prmt3. *Can. J. Chem.* **2013**, *91*, 605–612.